Chapter 6

Photodriven Sm(III)-to-Sm(II) Reduction for Catalytic Applications

Adapted from:

Johansen, C. M.†; Boyd, E. A.†; Tarnopol, D. E.; Peters, J. C. *J. Am. Chem. Soc.* **2024**. 146, 25456–25461. DOI: 1010.1021/jacs.4c10053.

† These authors contributed equally to this work.

6.1 Introduction

Samarium diiodide (SmI_2) is an exceptionally versatile single-electron reductant. The large and labile coordination sphere of Sm^{II} can recruit one or multiple substrates and additives to achieve selectivity in both organic synthesis and small-molecule reductions (Figure 6.1A).[1,2,3,4] However, SmI_2 is employed stoichiometrically in all but a few select cases[5,6,7,8] because its reactions typically terminate in the formation of highly stable Sm^{III}–alkoxide species. Catalytic regeneration of the Sm^{II} state requires abstraction of OR^- by a stoichiometric oxophile (EX) to generate a Sm^{III} species that can be reduced by a relatively mild reductant (Figure 1A). The difficulty associated with this transformation has been cited as a motivation for the development of a variety of alternative photo- and electrochemically driven methods for ketyl radical generation.[9,10,11,12,13]

Early strategies for reductive Sm catalysis relied on harsh combinations of halosilane oxophiles (R_3SiX) and low valent metals (Mg^0 for X = Cl; Zn^0 for X = I) or an applied electrochemical potential as the reductant.[14,15,16,17,18,19,20,21,22] In a collaborative effort with the Reisman laboratory, we recently disclosed comparatively mild silane-free thermal and electrochemical conditions for catalytic turnover of SmI_2 in reductive coupling of ketones and acrylates through combination of cationic Brønsted acids with either Zn^0 or an applied potential of −1.55 V vs $Fc^{+/0}$ ($Fc^{+/0}$ = ferrocenium/ferrocene; all potentials referenced to $Fc^{+/0}$).[23]

Given the growing interest in (metalla)photoredox catalysis,[24] photodriven strategies for $Ln^{III/II}$ catalysis remain surprisingly underexplored.[25,26] In a strategy recently showcased by the groups of Borbas[27] and Nemoto,[28] photosensitizers are incorporated into the secondary coordination spheres of Ln^{III} complexes (Ln = Sm, Eu; Figure 6.1B). Intramolecular oxidative quenching of the excited sensitizer by the Ln^{III} center produces a potent Ln^{II} reductant which can carry out a variety of transformations.

While this and other strategies show promise,[25,26,27,28] the chelating ligand platforms used thus far in photodriven $Ln^{III/II}$ catalysis (cryptands, bidentate phosphine oxides) restrict the coordination sphere and/or shift $E°(Ln^{III/II})$ to strongly negative potentials, belying direct

translation to the rich stoichiometric chemistry of $SmI_2(L)_n$ as an inner sphere reductant (L = solvent molecule, typically THF).

Lewis acidic metal ions are commonly used to template substrates in photodriven reductive coupling reactions.[10,29,30] Recently, in contrast to the use of photocatalysts, several Lewis acid-mediated photoreductions utilize the blue-light absorbing Hantzsch ester (HEH_2) as a photoreductant ($E(HEH_2^{+\bullet}/{}^*HEH_2) = -2.5$ V).[31,32,33,34] Photoexcited HEH_2 ($^*HEH_2$) carries out Cr^{III} reduction in a catalytic-in-Cr photodriven Nozaki–Hiyama–Kishi reaction (Figure 6.1C).[35] Alternatively, HEH_2 acts as a photoreductant in a $Gd(OTf)_3$-mediated Giese addition of an *N*-hydroxyphthalimide (NHPI) ester-derived alkyl radical into α,β-unsaturated ketones or lactone (Figure 6.1C).[36] In the latter study, an interaction between Gd and HEH_2 is observed, but Gd^{III} reduction to Gd^{II} is not accessible even by $^*HEH_2$.[23]

Based on these precedents we noted that $^*HEH_2$ should be capable of reducing Sm^{III}-species such as SmI_3 ($E°(SmI_3/(SmI_2 + I^-)) = -1.58$ V; Figure E.35). Because Sm and Gd are similar in size and oxophilicity, we envisioned that photoexcitation of HEH_2 bound to Sm^{III} could also result in intramolecular oxidative quenching to produce Sm^{II} (Figure 6.1D). Crucially, however, a more dynamic Sm-chromophore interaction might allow access to coordinatively unsaturated $SmI_2(L)_n$ species which could carry out inner-sphere reduction in a photodriven Sm-catalyzed cross-coupling reaction. Importantly, both HEH_2 and its $2H^+/2e^-$ oxidized congener, HE, are weak bases and are therefore compatible with the acidic conditions necessary for recovery of inactive Sm^{III}–OR species by protonolysis.

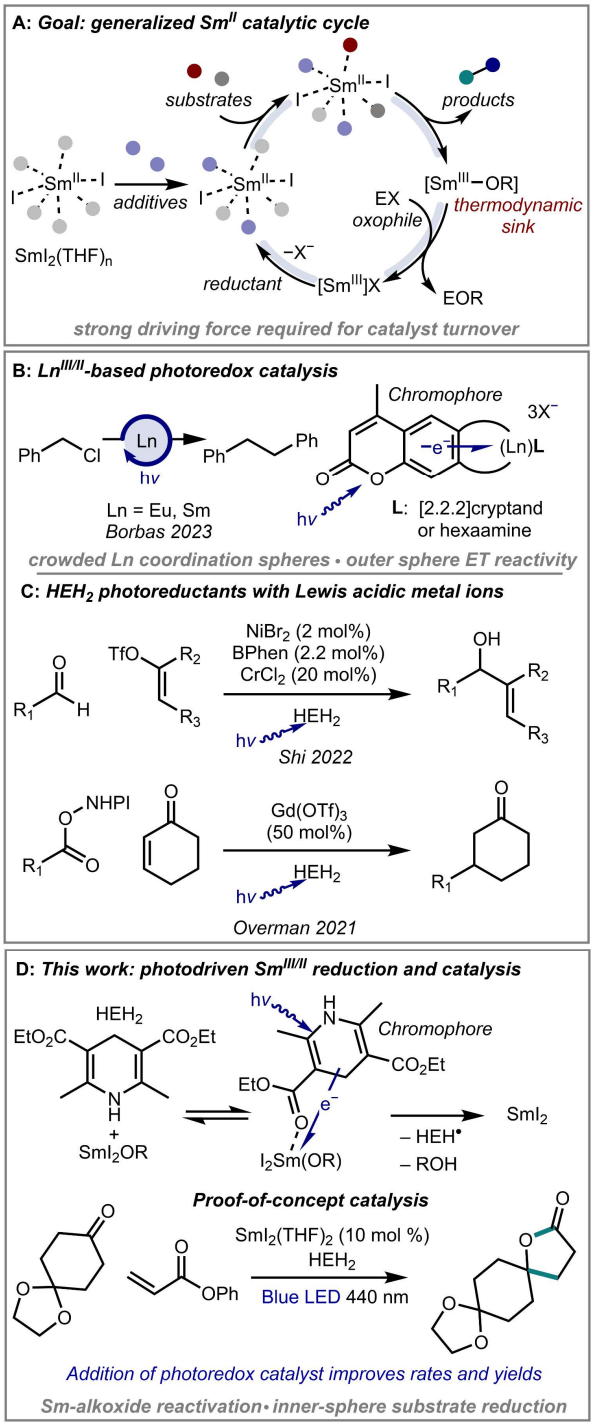

Figure 6.1. Summary of key challenges for Sm-turnover;[23] prior studies exploiting $Ln^{III/II}$ photochemistry and photoreductions with HEH_2 and Lewis acidic metals;[27,35,36] and this work describing photodriven generation of SmI_2.

6.2 Results

Gratifyingly, HEH_2 proved competent as a photoreductant for Sm^{III}-to-Sm^{II} conversion. Monitoring the UV-visible absorption spectrum of a solution of SmI_3 (2 mM), HEH_2 (60 mM) and 2,6-lutidine base (Lut, 60 mM) following irradiation at 440 nm for 5 min in THF reveals the characteristic profile of blue $SmI_2(THF)_n$ with λ_{max} at 555 and 618 nm (Figure 6.2A, left panel). Extended irradiation (120 minutes) results in increasing SmI_2 generation, with maximum yield ~25%. Interestingly, in the absence of base this reaction does not proceed (Figure E.17), likely due to rapid back-electron transfer (BET) between $HEH_2^{\bullet+}$ and SmI_2. However, $HEH_2^{\bullet+}$ can be deprotonated in the presence of base, circumventing BET.

We next evaluated conditions for photogeneration of $SmI_2(THF)_n$ from $Sm(O^iPr)_3$ as a model Sm^{III}-alkoxide. Irradiation of $Sm(O^iPr)_3$ (2 mM), tetra-*n*-heptylammonium iodide (^{n}Hep$_4$NI, 6 mM), and HEH_2 (60 mM) at 440 nm in THF shows no evidence of SmI_2 formation (Figure E.19). However, upon the addition of only 1.5 equiv of the acid *bis*-trifluoromethylsulfonylimide (HTFSI) to $Sm(O^iPr)_3$, $SmI_2(THF)_n$ is generated upon irradiation with ^{n}Hep$_4$NI and HEH_2 (Figure 6.2A, right panel). Parallel CV studies demonstrate that no SmI_3 is generated from $Sm(O^iPr)_3$ at this acid loading (Figure 6.2B, compare light and dark blue traces), and current attributable to Sm^{III} reduction (presumably of an intermediate mixture of solvated "$SmI(O^iPr)_2$" and "SmI_2O^iPr") does not onset until −2.3 V. In contrast to SmI_3, no external base is needed, suggesting that the Sm-bound alkoxide might additionally serve the role of deprotonating $HEH_2^{\bullet+}$ to avoid BET. UV-vis studies reveal that addition of the colorless Sm^{III}–O^iPr species (grey trace in Figure 6.2A) gives rise to a significantly red-shifted shoulder in the HEH_2 absorption profile (compare light and dark red traces in Figure 6.2A), consistent with pre-association.

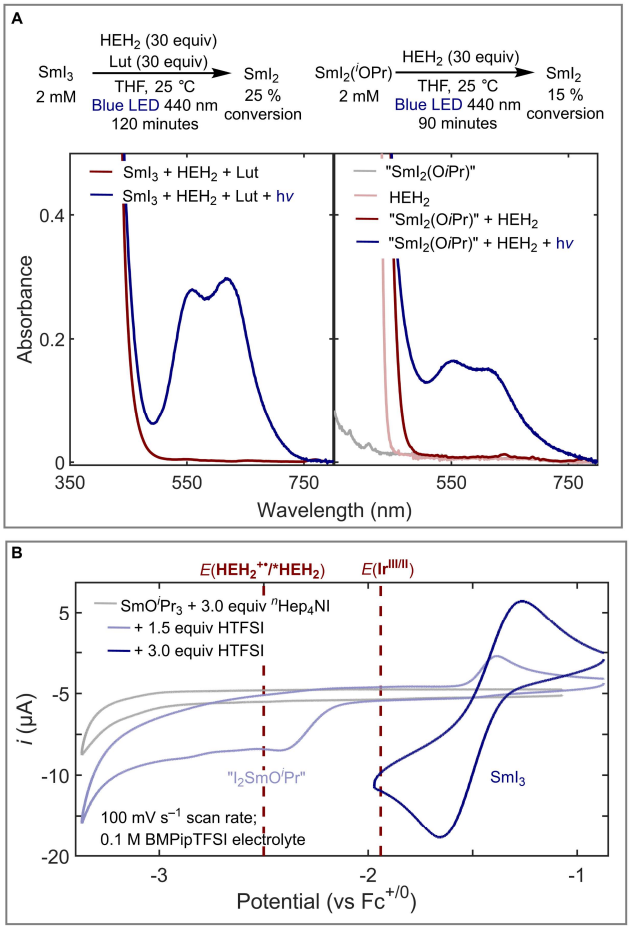

Figure 6.2. Photogeneration of SmI_2. (A) UV-vis spectra following photoreduction of SmI_3 (left) and $L_nSm(^iOPr)I_2$ to form SmI_2. CVs of $Sm(O^iPr)_3$ (2 mM) in the presence of iodide and proton sources in THF.

The modest yields and rates of these reactions motivated the study of Sm^{III} reduction with a photoredox catalyst to overcome the low quantum yield and excited state lifetime (220 ps in MeCN)[37] of HEH_2. We selected $[Ir(dtbbpy)(ppy)_2]^+$ ($[\mathbf{Ir^{III}}]^+$)[38] as a photosensitizer, which could undergo reductive quenching by a sacrificial electron donor to generate $\mathbf{Ir^{II}}$. $\mathbf{Ir^{II}}$ is thermodynamically capable of reducing SmI_3 to SmI_2 ($E°(\mathbf{Ir^{III/II}}) = -1.94$ V, Figure 6.2B and Figure E.36).

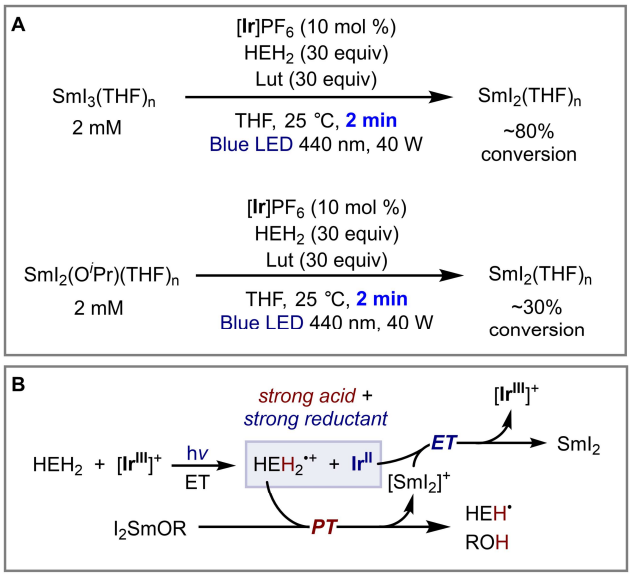

Figure 6.3. Photogeneration of SmI_2 with Ir photocatalyst. (A) Photoreductions of Sm^{III} species with $[Ir]PF_6$ photocatalyst. (B) Rationale for net photoinduced proton- and electron-transfer from HEH_2 to $[Sm^{III}–OR]$ species.

Irradiating SmI_3 or SmI_2O^iPr (2 mM) with $[\mathbf{Ir^{III}}]PF_6$ (0.2 mM), HEH_2 (60 mM) as sacrificial reductant, and Lut (60 mM) rapidly generates SmI_2 (80% or 30% conversion in 2 min, Figure 6.3A). Again, the weak base Lut enhances the process (Figures E.20-E.21).

The accelerated reduction of SmI_2O^iPr is curious, as electron transfer from $\mathbf{Ir^{II}}$ to this Sm^{III} species is uphill by 400 mV (Figure 6.2B). A rationale for these observations is provided in Figure 6.3B: reductive quenching of $*[\mathbf{Ir^{III}}]^+$ by HEH_2 generates not only the strong reductant $\mathbf{Ir^{II}}$, but also the strong acid $HEH_2^{\bullet+}$ (pK_a −1 in MeCN),[39,40] the combination of which can carry out net proton-coupled electron transfer to $Sm^{III}–O^iPr$.[41] Proton transfer from $HEH_2^{\bullet+}$ to a $Sm^{III}–O^iPr$ species, likely via proton relay mediated by Lut, liberates ^{i}PrOH and $[SmI_2]^+$.[42] The latter can then be reduced to SmI_2 by $\mathbf{Ir^{II}}$.

Development of Sm-catalysis leveraging diverse ligand coordination to modulate reactivity is an attractive goal. Exploration of Sm^{II} generation in the presence of potential coligands was carried out pursuant to these interests.

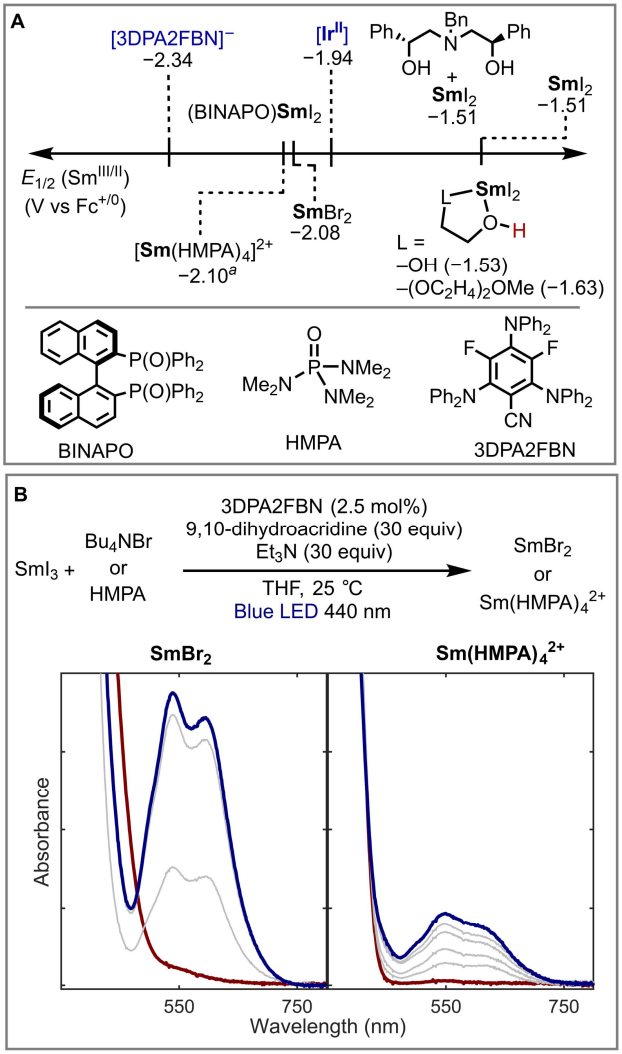

Figure 6.4. Photogeneration of Sm^{II} with alternate ligands. (A) Ligand coordinated Sm-species generated by a photoredox approach. See Appendix E for relevant electrochemical data. Choice of a sufficiently reducing photocatalyst remains crucial to observe Sm^{II}. (B) UV-vis spectra following photogeneration of $SmBr_2$ and $Sm(HMPA)_4^{2+}$.

Satisfyingly, Sm^{II} is readily photogenerated from SmI_3 by $[\mathbf{Ir^{III}}]^+$ and quencher (HEH_2 or Et_3N) in the presence of several protic additives (ethylene glycol, *N,N*-dimethylaminoethanol, Figures E.23-E.24),[3,43,44,45] including a chiral aminediol (Figure 6.4A, Figure E.25) that has been utilized in several enantioselective SmI_2 transformations.[46,47,48]

The reduction potential and reactivity of Sm^{II} is highly sensitive to coordination of Lewis-basic additives (HMPA, Br^-; Figure 6.4A).[49] While [$\mathbf{Ir^{II}}$] is insufficiently reducing to access such species, the more reducing photocatalyst 3DPA2FBN, [50] when paired with the more reducing quencher 9,10-dihydroacridine and Et_3N as base, mediates generation of both $SmBr_2$ and $Sm(HMPA)_4^{2+}$ (Figure 6.4B). 3DPA2FBN also facilitates Sm^{III} reduction and binding to the chiral BINAPO ligand (Figures 6.4A and E.34).[51,52]

Having established two different photochemical approaches to Sm^{II} generation, we targeted an intermolecular ketone-acrylate coupling as a model reaction to benchmark photodriven Sm-catalysis (Table 6.1). This reaction is representative of the qualities that set SmI_2 apart as a stoichiometric reductant. Inner sphere electron transfer to one or both of the carbonyl substrates is obligatory based on comparison of outer-sphere reduction potentials.[23] Importantly, a Sm-alkoxide is generated as the byproduct of lactonization, enabling evaluation of the ability of a set of conditions to overcome this critical barrier to generalizable Sm catalysis.

Irradiation of ketone **1** (0.04 mmol), phenyl acrylate (2 equiv), and $SmI_2(THF)_2$ (10 mol %) in the presence of HEH_2 (4.0 equiv) in 2-MeTHF (0.02 M) at 440 nm for 90 min yields lactone **2** in 76% yield (Table 6.1, entry 1, method A). Addition of a photoredox catalyst ([**Ir**]PF_6, 1 mol%) with pyridine (2 equiv) results in an increase in yield to 89% (Entry 1, method B). Light and Sm were required for catalytic formation of **2** by either method (entries 3 and 4). $Sm(OTf)_3$ is a competent precatalyst with 50 mol% MgI_2 included as an iodide source (entry 4). Substitution of $Gd(OTf)_3$ for $Sm(OTf)_3$ results in trace product formation, supporting a key role for Sm^{II} in catalysis (entry 5).

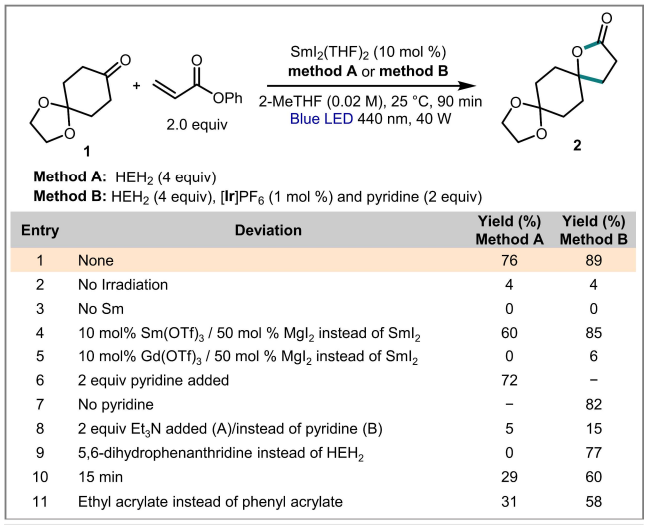

Entry	Deviation	Yield (%) Method A	Yield (%) Method B
1	None	76	89
2	No Irradiation	4	4
3	No Sm	0	0
4	10 mol% $Sm(OTf)_3$ / 50 mol % MgI_2 instead of SmI_2	60	85
5	10 mol% $Gd(OTf)_3$ / 50 mol % MgI_2 instead of SmI_2	0	6
6	2 equiv pyridine added	72	–
7	No pyridine	–	82
8	2 equiv Et_3N added (A)/instead of pyridine (B)	5	15
9	5,6-dihydrophenanthridine instead of HEH_2	0	77
10	15 min	29	60
11	Ethyl acrylate instead of phenyl acrylate	31	58

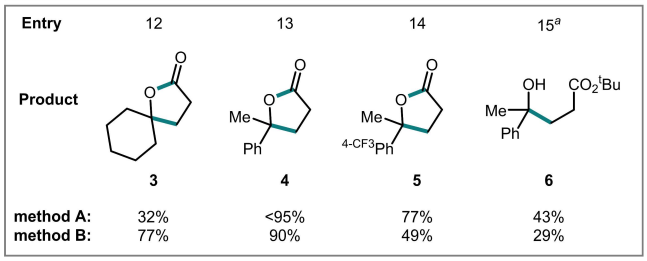

	12	13	14	15[a]
method A:	32%	<95%	77%	43%
method B:	77%	90%	49%	29%

Table 6.1. Photodriven Sm-catalyzed coupling of ketones and phenyl acrylate to form lactone products. Yields were determined by ^{1}H NMR analysis. For additional reaction data, see Table E.2. [a]*tert*-butyl acrylate used as coupling partner; lactonization observed only upon acidic workup.

Both methods are competent in the presence/absence of pyridine (entries 1, 6, and 7), but yields are greatly diminished in the presence of a stronger base (Et_3N, entry 8). This suggests that the dynamics of Sm-alkoxide protonation play an important role in turnover.[23] Interestingly, the use of a dihydropyridine without carbonyl groups, 5,6-dihydrophenanthridine, only shows product formation with [**Ir**]$^+$ (entry 9). In the absence of Ir, the specific interaction between Sm and HEH_2 appears to be required. The Ir-catalyzed reaction is also faster, achieving 60% conversion in 15 minutes, compared to 29% by method A (entry 10).

Methods A and B were tested against alternative coupling partners to assess their relative efficacies. When using less activated substrate pairs (aliphatic ketones and alkyl acrylates, entries 1, 11 and 12), method B is favored, perhaps because these slower cross-couplings require rapid Sm^{III}-to-Sm^{II} conversion. Method A is preferred when using aryl

ketones (entries 13-15), as method B gives considerable pinacol-coupled side-products (Table E.3). With method A, selective inner-sphere photogeneration of Sm^{II} by Sm^{III}–HEH_2 may favor Sm^{II}-mediated cross-coupling, while with method B background Ir-mediated substrate reduction to homocoupled products can dominate.

A proposed mechanism for this photodriven lactonization reaction (by method A) is presented in Figure 6.5. The mechanism can be divided into two parts, a photoreduction side in which Sm^{III} is reduced to Sm^{II}, and a SmI_2 cross-coupling side where the organic substrates are coupled. Starting from $SmI_2(OPh)$, coordination to HEH_2 (as demonstrated in Figure 6.2A) followed by excitation to $*HEH_2$ allows for the proton and electron transfer required to generate SmI_2, with PhOH and $HEH^{\bullet}$ as additional products. Subsequently, SmI_2 couples the acrylate and ketone to form a radical intermediate.[53,54] $HEH^{\bullet}$ is capable of reducing this intermediate as a potent H-atom donor, although alternative schemes for reduction of the radical intermediate can be envisioned (Figure E.45). Following reduction and lactonization, **2** is formed along with $SmI_2(OPh)$.

With $[\mathbf{Ir}]^+$, a similar mechanism is proposed, differing in the regeneration of Sm^{II}, which can be regenerated from Sm^{III}-alkoxide as depicted in Figure 6.3B (see Figure E.46 for full scheme).

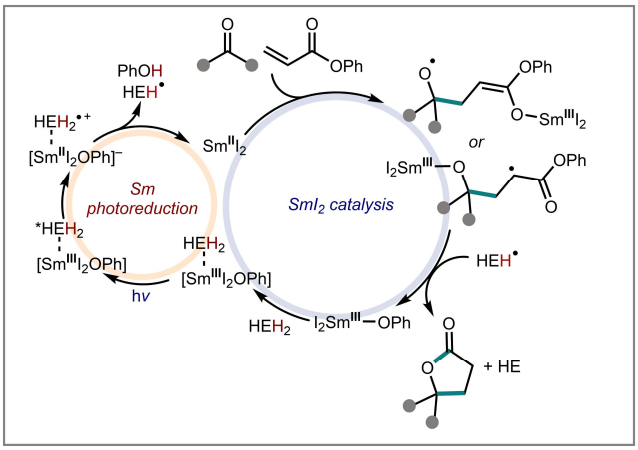

Figure 6.5. Proposed mechanism of Sm cross-coupling under Ir-free conditions (method A).

6.3 Conclusions

In summary, we have demonstrated photodriven generation of $SmI_2(THF)_2$ from Sm^{III} precursors using both a photoreductant and a photoredox catalyst. These conditions translate to proof-of-concept photodriven reductive Sm-catalyzed ketone-acrylate coupling. Distinct from reported methods, photodriven Sm-catalysis occurs in the absence of competing Lewis-acidic metal additives and byproducts (e.g., Mg^{2+} and Zn^{2+} salts),[14,15,16,17,18,19,20,21,22,23] which may be of utility in development of Sm-catalysis with ligands.[3,18,43,46,47,48,49,50,51] These findings are anticipated to facilitate applications of Sm-catalysis beyond the types of thermally driven transformations studied thus far.

6.4 Cited references

1. Girard, P.; Namy, J. L.; Kagan, H. B. *J. Am. Chem. Soc.* **1980**. 102, 2693–2698.
2. Szostak, M.; Fazakerley, N. J.; Parmar, D.; Procter, D. J. *Chem. Rev.* **2014**. 114, 5959–6039.
3. Ashida, Y.; Arashiba, K.; Nakajima, K.; Nishibayashi, Y. *Nature* **2019**. 568, 536–540.
4. Lee, C. C.; Hu, Y.; Ribbe, M. W. *Angew. Chem. Int. Ed.* **2015**. 54, 1219–1222.
5. Net redox-neutral SmI_2-catalyzed radical relay processes have been explored; see the following and refs 5-8: Huang, H.-M.; McDouall, J. J. W.; Procter, D. J. *Nat. Catal.* **2019**. 2, 211–218.
6. Agasti, S.; Beattie, N. A.; McDouall, J. J. W.; Procter, D. J. *J. Am. Chem. Soc.* **2021**. 143, 3655–3661.
7. Agasti, S.; Beltran, F.; Pye, E.; Kaltsoyannis, N.; Crisenza, G. E. M.; Procter, D. J. A *Nat. Chem.* **2023**. 15, 535–541.
8. Mansell, J. I.; Yu, S.; Li, M.; Pye, E.; Yin, C.; Beltran, F.; Rossi-Ashton, J. A.; Romano, C.; Kaltsoyannis, N.; Procter, D. J. *J. Am. Chem. Soc.* **2024**. 146, 12799–12807.

9. Edgecomb, J. M.; Alektiar, S. N.; Cowper, N. G. W.; Sowin, J. A.; Wickens, Z. K. *J. Am. Chem. Soc.* **2023**. 145, 20169–20175.
10. Lee, K. N.; Lei, Z.; Ngai, M.-Y. *J. Am. Chem. Soc.* **2017**. 139, 5003–5006.
11. Derosa, J.; Garrido-Barros, P.; Peters, J. C. *Inorg. Chem.* **2022**. 61, 6672–6678.
12. Tarantino, K. T.; Liu, P.; Knowles, R. R. *J. Am. Chem. Soc.* **2013**. 135, 10022–10025.
13. Seo, H.; Jamison, T. F. *Org. Lett.* **2019**. 21, 10159–10163.
14. Corey, E. J.; Zheng, G. Z. *Tetrahedron Lett.* **1997**. 38, 2045–2048.
15. Nomura, R.; Matsuno, T.; Endo, T. *J. Am. Chem. Soc.* **1996**. 118, 11666–11667.
16. Aspinall, H. C.; Greeves, N.; Valla, C. *Org. Lett.* **2005**. 7, 1919–1922.
17. Sun, L.; Sahloul, K.; Mellah, M. *ACS Catal.* **2013**. 3, 2568–2573.
18. Maity, S.; Flowers, R. A. *J. Am. Chem. Soc.* **2019**. 141, 3207–3216.
19. Hébri, H.; Duñach, E.; Heintz, M.; Troupel, M.; Périchon, J. *Synlett* **1991**. 1991, 901–902.
20. Hebri, H.; Duñach, E.; Périchon, J. *J. Chem. Soc., Chem. Commun.* **1993**. 6, 499–500.
21. Hebri, H.; Duñach, E.; Périchon, J. *Synth. Commun.* **1991**. 21, 2377–2382.
22. Espanet, B.; Duñach, E.; Périchon, J. *Tetrahedron Lett.* **1992**. 33, 2485–2488.
23. Boyd, E. A.; Shin, C.; Charboneau, D. J.; Peters, J. C.; Reisman, S. E. *Science* **2024**. 385, 837-843.
24. Chan, A. Y.; Perry, I. B.; Bissonnette, N. B.; Buksh, B. F.; Edwards, G. A.; Frye, L. I.; Garry, O. L.; Lavagnino, M. N.; Li, B. X.; Liang, Y.; Mao, E.; Millet, A.; Oakley, J. V.; Reed, N. L.; Sakai, H. A.; Seath, C. P.; MacMillan, D. W. C. *Chem. Rev.* **2022**. 122, 1485–1542.
25. Meyer, A. U.; Slanina, T.; Heckel, A.; König, B. *Chem. Eur. J.* **2017**. 23, 7900–7904.

26. Jenks, T. C.; Bailey, M. D.; Hovey, J. L.; Fernando, S.; Basnayake, G.; Cross, M. E.; Li, W.; Allen, M. J. *Chem. Sci.* **2018**. 9, 1273–1278.
27. Tomar, M.; Bhimpuria, R.; Kocsi, D.; Thapper, A.; Borbas, K. E. *J. Am. Chem. Soc.* **2023**. 145, 22555–22562.
28. Kuribara, T.; Kaneki, A.; Matsuda, Y.; Nemoto, T. *J. Am. Chem. Soc.* **2024**. 146, 20904-20912.
29. Yoon, T. P. *Acc. Chem. Res.* **2016**. 49, 2307–2315.
30. Huang, X.; Luo, S.; Burghaus, O.; Webster, R. D.; Harms, K.; Meggers, E. *Chem. Sci.* **2017**. 8, 7126–7131.
31. Jung, J.; Kim, J.; Park, G.; You, Y.; Cho, E. J. *Adv. Synth. Catal.* **2016**. 358, 74–80.
32. Ohnishi, Y.; Kagami, M.; Ohno, A. *Chem. Lett.* **1975**. 4, 125–128.
33. Johansen, C. M.; Boyd, E. A.; Peters, J. C. *Science Advances* **2022**. 8, eade3510.
34. Ji, C.-L.; Han, J.; Li, T.; Zhao, C.-G.; Zhu, C.; Xie, J. *Nat. Catal.* **2022**. 5, 1098–1109.
35. Liu, Y.; Lin, S.; Zhang, D.; Song, B.; Jin, Y.; Hao, E.; Shi, L. *Org. Lett.* **2022**. 24, 3331–3336.
36. Pitre, S. P.; Allred, T. K.; Overman, L. E. *Org. Lett.* **2021**. 23, 1103–1106.
37. Deng, G.; Xu, H.-J.; Chen, D.-W. *J. Chem. Soc., Perkin Trans. 2* **1990**. 7, 1133–1137.
38. Slinker, J. D.; Gorodetsky, A. A.; Lowry, M. S.; Wang, J.; Parker, S.; Rohl, R.; Bernhard, S.; Malliaras, G. G. *J. Am. Chem. Soc.* **2004**. 126, 2763–2767.
39. Shen, G.-B.; Fu, Y.-H.; Zhu, X.-Q. *J. Org. Chem.* **2020**. 85, 12535–12543.
40. Schmittel, M.; Burghart, A. *Angew. Chem. Int. Ed.* **1997**. 36, 2550–2589.
41. Boyd, E. A.; Peters, J. C. *J. Am. Chem. Soc.* **2022**. 144, 21337–21346.
42. Analogous net proton-coupled electron transfer to Ti(IV)-alkoxide species to generate Ti(III) has been proposed in photodriven Ti redox catalysis: Gualandi, A.;

Calogero, F.; Mazzarini, M.; Guazzi, S.; Fermi, A.; Bergamini, G.; Cozzi, P. G. *ACS Catal.* **2020**. 10, 3857–3863.

43. Chciuk, T. V.; Flowers, R. A. *J. Am. Chem. Soc*. **2015**. 137, 11526–11531.
44. Kolmar, S. S.; Mayer, J. M. *J. Am. Chem. Soc.* **2017**. 139, 10687–10692.
45. Boekell, N. G.; Bartulovich, C. O.; Maity, S.; Flowers, R. A. I. *Inorg. Chem.* **2023**. 62, 5040–5045.
46. Kern, N.; Plesniak, M. P.; McDouall, J. J. W.; Procter, D. J. *Nature Chem.* **2017**. 9, 1198–1204.
47. Evans, D. A.; Nelson, S. G.; Gagne, M. R.; Muci, A. R. *J. Am. Chem. Soc.* **1993**. 115, 9800–9801.
48. Wang, Y.; Zhang, W.-Y.; Yu, Z.-L.; Zheng, C.; You, S.-L. *Nat. Synth* **2022**. 1, 401–406.
49. Miller, R. S.; Sealy, J. M.; Shabangi, M.; Kuhlman, M. L.; Fuchs, J. R.; Flowers, R. A. *J. Am. Chem. Soc.* **2000**. 122, 7718–7722.
50. Speckmeier, E.; Fischer, T. G.; Zeitler, K. *J. Am. Chem. Soc.* **2018**. 140, 15353–15365.
51. Mikami, K.; Yamaoka, M. *Tetrahedron Lett.* **1998**. 39, 4501–4504.
52. CV experiments suggest that speciation of 1:1 SmI_3:BINAPO is a complex mixture with $Sm^{III/II}$ redox waves negative of −2 V (Figure E.43).
53. Substrate coupling could be initiated either by ketone or acrylate reduction, leading to either an α-ester radical or an alkoxy radical intermediate, respectively, following addition to the corresponding coupling partner. In the case of difficult-to-reduce ketone substrates such as **1**, neither pathway can be reliably ruled out. See the following and ref 54 for detailed examination of this mechanistic question: Hansen, A. M.; Lindsay, K. B.; Sudhadevi Antharjanam, P. K.; Karaffa, J.; Daasbjerg, K.; Flowers, R. A.; Skrydstrup, T. *J. Am. Chem. Soc.* **2006**. 128, 9616–9617.
54. Sono, M.; Hanamura, S.; Furumaki, M.; Murai, H.; Tori, M. *Org. Lett.* **2011**. 13, 5720–5723.